coatings

MDPI

*Article*

# Influence of Graphene Oxide Additions on the Corrosion Resistance of a Rust Converter Primer

**Belén Díaz, Xosé Ramón Nóvoa, Carmen Pérez * and Miguel Rodríguez-Morgado**

CINTECX, Universidade de Vigo, ENCOMAT Group, 36310 Vigo, Spain; belenchi@uvigo.es (B.D.); rnovoa@uvigo.es (X.R.N.); miguelromorgado@gmail.com (M.R.-M.)
* Correspondence: cperez@uvigo.es

**Abstract:** Graphene oxide (GO) has attractive properties, such as a two-dimensional structure. Because of its hydrophilic characteristic, well-dispersed aqueous solutions are attained. Thus, it is easily incorporated into waterborne resins. For these reasons, in the last years GO nanoparticles have been added to polymers, improving corrosion resistance. This work is focused on the performance of a commercial rust converter (RC) doped with five different RC:GO ratios, namely, 1:0; 1:0.3; 1:0.6; 1:0.9; 1:1.2 (%v/v). The X-ray diffraction technique is used to illustrate the effect of RC and RC + GO additions in the iron oxides. Zeta-potential measurements are performed to assess the surface charge of the GO particles. The corrosion resistances of the rusted samples coated with the five rust converter formulations are studied. The electrochemical impedance spectroscopy (EIS) technique and an electrical equivalent circuit are utilized to explain the experimental results. Additionally, it is found that the optimal RC:GO ratio is between 1:0.3 and 1:0.6. The better corrosion resistance reached is that of the RC:0.3GO ratio.

**Keywords:** rusted steel; rust converter; graphene oxide; corrosion resistance



**Citation:** Díaz, B.; Nóvoa, X.R.; Pérez, C.; Rodríguez-Morgado, M. Influence of Graphene Oxide Additions on the Corrosion Resistance of a Rust Converter Primer. *Coatings* **2022**, *12*, 345. https://doi.org/10.3390/coatings12030345

Academic Editors: Fernando Pedraza and Ludmila B. Boinovich

Received: 9 February 2022
Accepted: 4 March 2022
Published: 6 March 2022



## 1. Introduction

The use of paints for the protection of steel structures is one of the most common strategies to mitigate corrosion. The success of this procedure is strongly dependent on the surface preparation of the metal. The optimum condition implies complete removal of rust; however, this is not always possible due to diverse reasons such as the inaccessibility of the elements, the repairing of large structures where conventional rust cleaning methods are expensive, or environmental constraints [1]. In these situations, an attractive alternative is the stabilization of the oxide layer before painting by the use of rust converters, which essentially consist of chemical formulations able to transform the iron oxides into a more compact and adherent layer. These compounds are designed to be applied on corroded surfaces [2,3]. The commercial rust converter (RC) formulations include two main components: the active one that reacts with the rust to generate new less reactive compounds, and the polymeric component responsible for the continuous film formation [3]. Most common formulations are based on tannic or phosphoric acids [4–8], and more recently they are also based on gallic acid [9–11] as an active component. Although they represent environmentally good alternatives to contaminant pretreatments, their efficiency is subject to controversy. Several parameters condition the final result, for example, the nature of the rust to be converted (composition, age, or thickness) that is determined by the type of atmosphere (presence of aggressive electrolytes, pH, etc.) [8,12,13], and the contact time between the RC and the rust [14]. This latter aspect is related to the chemical nature of the active component in the RC. There is a general agreement that the stabilization of the rust is based on the ability of these compounds to react with the iron oxides/hydroxides creating a passive layer [15] that can be accompanied by a sealing effect [16]. However, this protection is limited or even not present, since the interaction between the oxides and the rust converter solutions affects only the outermost rust surface [4,17,18]. Ocampo et al.

suggest that their effect can be even harmful in the case of high chloride contamination [1]. Thus, developing new RC formulations with good long-term protection is a challenging task. To our best knowledge, few studies deal with this aspect [10,19].

The incorporation of corrosion inhibitors to the commercial RC may be an alternative strategy, following the same route as employed in traditional paint formulations. In a previous work [11], we demonstrated the benefit provided by the addition of oxide (GO) to a commercial rust converter. The choice of GO as a pigment for anticorrosive coatings was based on some advantageous features that it possesses. It is a two-dimensional nanomaterial; i.e., it has a very high aspect ratio, thus it would provide a good barrier effect. Besides, it has a hydrophilic character due to the oxygen-containing functional groups (epoxy and hydroxyl at the planar surface, and carbonyl, carboxyl, ester, ether, phenol, among others, at the edges). This characteristic encourages the stabilization of the aqueous GO dispersions and also provides active points to be covalently bonded to other species [20,21]. Functionalization of the GO is a common approach used to improve the compatibility of the GO with the polymeric matrix, thus avoiding dispersion or agglomeration problems [22,23]. However, the experimental procedure usually is complex, which restricts its implementation on an industrial scale. In our proposal, the GO was added as an aqueous dispersion over commercial water-based RC, which simplifies the mixing process and the dispersion of the mixture was good [11]. Using a similar procedure, the present work is focused on the optimization of the GO concentration that provides the best anticorrosive properties of the commercial rust converter.

## 2. Materials and Methods

Mild steel samples with 80 mm × 30 mm × 1 mm dimensions and nominal chemical composition (wt.%): C (0.096), Mn (0.350), Si (0.183), Cr (0.123), Ni (0.161), Mo (0.06), P (0.022), S (0.033), Co (0.046), Sn (0.041), and Fe (balance), were degreased using soapy water and afterward rinsed with deionized water and dried. The clean steel plates were prerusted in a humidity chamber at 100% relative humidity and room temperature until the generation of a uniform rust layer; this process takes about two weeks. The corroded samples were brushed to remove the loose rust before applying the RC formulations. The detached oxides were collected and dried in a furnace at about 40 °C. They were then milled to obtain a fine powder and dry-stored to perform further experiments.

The commercial rust converter named Oroprimer® 440 (produced by Oropal, Irurena Group, Azpeitia, Spain) was used. It is a water emulsion based on vinyl chloride–acrylic ester copolymer, with gallic acid as the active component; the density is 1.2 g. $mL^{-1}$ and the total solid content is 50%. The graphene oxide employed is a GO water dispersion with 0.4 wt.% concentration from Graphenea® (Graphenea Inc., Boston, MA, USA). Five RC:GO ratios, 1:0; 1:0.3; 1:0.6; 1:0.9; and 1:1.2 (%v/v), were studied. The mixtures were then sonicated for 2 min to obtain a homogenous suspension that was applied by brush on the rusted steel samples and cured for 48 h at room temperature. Figure 1 illustrates the aspect of the rusted steel samples coated with the RC/GO formulations. As can be appreciated, a thin and uniform film was obtained, the average thickness was 42 ± 2.6 μm.

The surface charge of the graphene oxide particles when they are in contact with the gallic acid was determined by zeta potential measurements. For that, gallic aqueous solutions (15 mg·$mL^{-1}$) with different concentrations of GO, 0.28 mg·$mL^{-1}$, 0.58 mg·$mL^{-1}$, 0.74 mg·$mL^{-1}$ and 0.92 mg·$mL^{-1}$, were prepared. These concentrations were determined taking into account that the amount of gallic acid in the rust converter is around 10% (information provided by the manufacturer) and the RC/GO ratios of 1:0.3; 1:0.6; 1:0.9 and 1:1.2 proposed in this study. The measurements were performed using a Malvern Zetasizer NanoSizer NanoZS® (Malvern Panalytical, Worcestershire, UK) instrument. The reproducibility was verified by performing a minimum of 10 measurements per set. The zeta potential was calculated from the electrophoretic mobility using the Smoluchowski model, wherein the thickness of the electrical double layer is assumed to be small in comparison with the particle size.

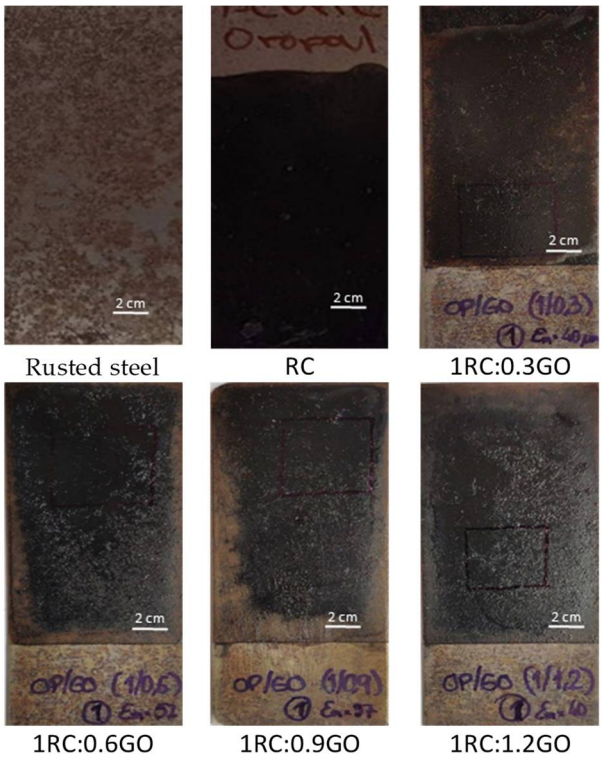


**Figure 1.** Pictures of rusted steel samples that were coated using the different RC:GO ratios, with 80 mm × 30 mm × 1 mm dimensions.

The interaction between the rust converter and iron oxides was assessed by the X-ray diffraction (XRD) technique. Samples were prepared by mixing the rust powder with the RC/GO formulations. After drying, these were again milled to obtain a fine powder. The equipment employed was an X-ray diffractometer PANalytical X'Pert® (Malvern Panalytical, Worcestershire, UK) powder with the monochromatic $CuK_\alpha$ radiation (λ = 1.5 Å) from 2θ = 15° to 2θ = 70°.

The protective features of the RC/GO formulations applied on the rusted steels were assessed using the electrochemical impedance spectroscopy (EIS) technique. The electrochemical cell was a three-electrode arrangement, wherein the working electrode was the coated steel defining a working area of S = 1 $cm^2$, the counter electrode was a large graphite sheet (28 $cm^2$), and a saturated calomel electrode (SCE) was used as the reference electrode. The electrolyte was 0.06 M NaCl solution confined in a volume of about 80 mL. The reason to choose this low chloride concentration is based on the characteristics of the rust converter; it is designed as a primer coat, thus, it has poor barrier properties. The use of a low aggressive electrolyte allows tracking the behavior of the different formulations at long immersion times. The equipment was an Autolab 30 potentiostat from Ecochemie® (Metrohm AG, Herisau, Switzerland), at null DC current and applying a 10 $mV_{rms}$ sinusoidal amplitude. The frequency ranged from 100 kHz to 10 mHz, with 7 points per decade. At least three samples were tested for each system to verify the reproducibility.

## 3. Results and Discussion

### *3.1. Surface Charge of the Graphene Oxide Particles*

The zeta-potential measurements provide useful information about the stability of the GO suspensions in the rust converter. For comparative purposes, zeta-potential measurements of GO aqueous solutions without acid gallic were also performed. The results are depicted in Figure 2.

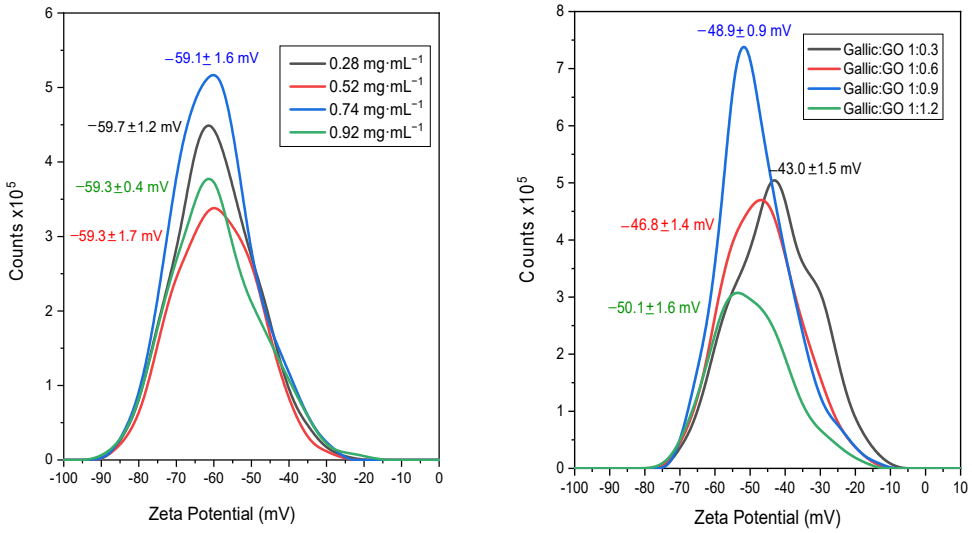


**Figure 2.** Zeta-potential distributions of GO in (**a**) aqueous solutions and (**b**) aqueous gallic acid solutions. The concentrations correspond to the amount of GO in the RC/GO formulations studied.

Figure 2a shows the zeta-potential values of the GO aqueous suspensions at different concentrations. The low value obtained, −59 mV, indicate very stable suspensions, regardless of the concentration. It is widely accepted that absolute values higher than 30 mV lead to stable suspensions due to interparticle electrostatic repulsion [24]. On the other hand, the negative zeta potential values are owing to the electronegative functional groups present in the GO particles [25]. The effect of the gallic acid is shown in Figure 2b. The zeta-potential values remain well below −30 mV, which confirms the stability of these suspensions. However, the recorded values are less negative than those in aqueous solutions. The reason should be twofold: on one hand, the parent solution is a concentrated gallic acid solution (15 mg·mL$^{-1}$) with high ionic strength, which reduces the thickness of the double layer and the repulsive forces, so that increases the zeta potential [26]. On the other hand, the partial protonation of the functional groups of the GO particles neutralizes the surface negative charge. This protonation seems more effective in dilute solutions, where the amount of GO particles is lower. This fact can explain the tendency for zeta potential to decrease when the GO concentration increases.

### *3.2. X-ray Characterization*

The interaction between the graphene oxide particles and the commercial rust converter was also verified by XRD. Figure 3 shows a detail of the X-ray diffractograms corresponding to the lowest and highest RC:GO ratios tested, in which the more characteristic diffraction peaks of gallic acid are depicted. The intensity of those peaks is markedly lower when the amount of GO is higher, which suggests certain interaction between both species. This result is not unexpected considering the reducing character of the gallic acid and is in agreement with the work of Li et al., in which the GO is reduced by gallic acid; this acts not only as a reductant agent but also as a stabilizer of the reduced graphene oxide (rGO) suspensions that were obtained [27]. The X-ray pattern of pure graphene oxide is also included, with a characteristic peak centered at 2θ = 10°. As can be seen, this peak is not observed in any of the RC/GO mixtures, owing to the low GO amount in the formulations. It also corroborates the interaction between gallic acid and GO. Similar results were obtained using other polyphenols such as tannic acid [28].

The XRD technique was also used to characterize the iron oxides/hydroxides generated and several mixtures of rust with the RC. The diffractograms obtained for the rust powder and its combination with the RC are shown in Figure 4. The main crystalline compounds identified were lepidocrocite γ-FeO(OH) (ref. code 00-008-0098) and mag-

netite $Fe_3O_4$ (ref. code 00-019-0629); traces of goethite, $\alpha$-FeO(OH) (ref. code 00-029-0713) were also detected. The same species were found by other researchers, even though the relative amounts may differ depending on the conditions in which the rust was generated [16,29,30]. The main crystalline compounds were also clearly detected when the rust was in contact with the RC, although there was a significant decrease in the intensity of the peaks. This expected result confirms the interaction between the rust converter and the iron oxides/hydroxides, and is in good agreement with other researchers [1,13].

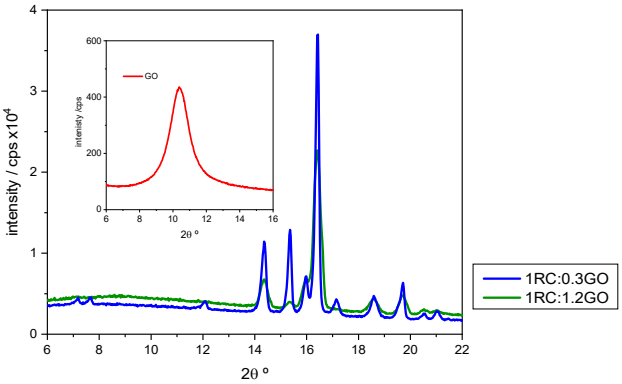


**Figure 3.** Detail of the X-ray patterns corresponding to 1RC:0.3GO and 1RC:1.2GO ratios. The X-ray pattern of GO is given in the insert.

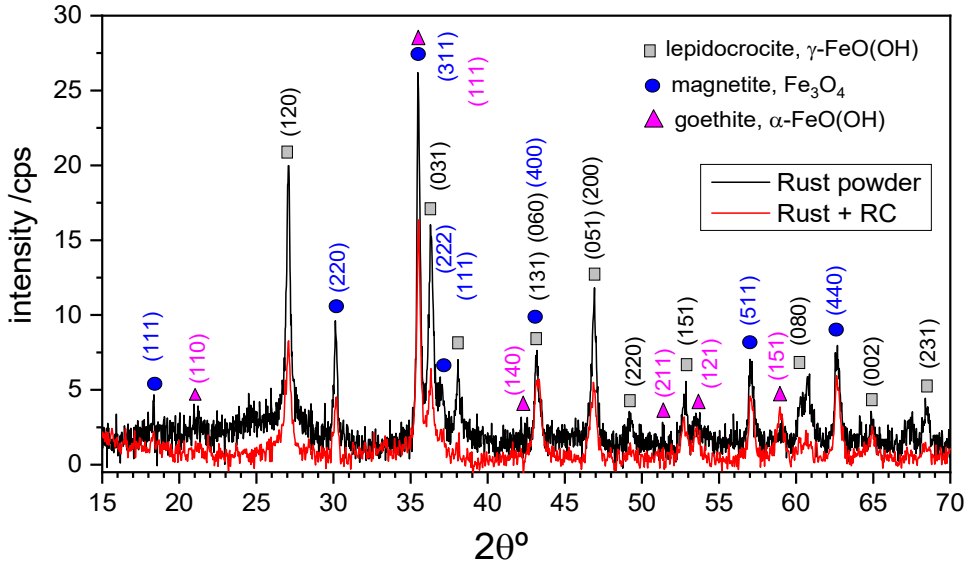


**Figure 4.** X-ray patterns obtained for dried rust powder and rust + RC mixture after being in contact for 15 days. The identification of the main crystalline compounds is also included together with the diffraction planes in each identified species based on refs. [31–33].

When the rust is mixed with the RC/GO formulations the intensity of the peaks also decreases, as Figure 5 illustrates. Although there is no clear tendency, the reduction is broadly less pronounced in the RC + GO blends. Even though it is not totally understood, this behavior may be related to the previous interaction between the gallic acid and the GO; thus, a smaller amount of the active component of the RC (i.e., gallic acid) would be available to react with the rust. As expected, the GO peak is not observed, as was already evident in the RC/GO mixtures.

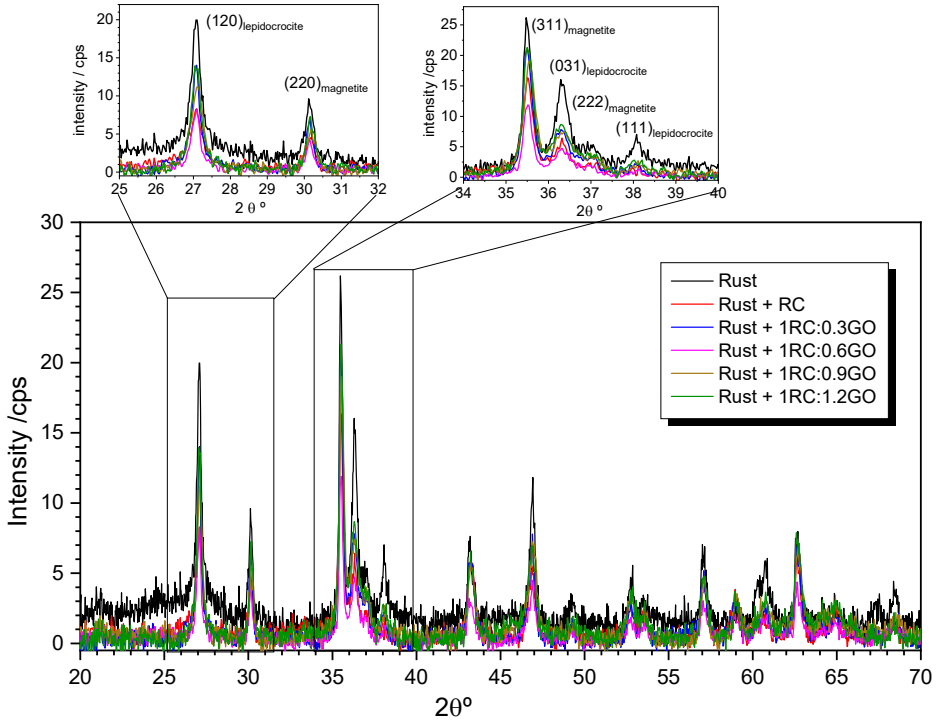


**Figure 5.** X-ray diffractograms obtained for rust powder and the different RC/GO mixtures tested, after being in contact for 15 days.

### *3.3. Electrochemical Study of Rusted Steel Coated with the RC/GO Treatments*

EIS measurements were performed to assess the corrosion resistance of the RC/GO formulations, and some examples are shown in Figure 6.

As can be seen, the better behavior corresponds to 1RC:0.3GO ratio not only initially but also for long immersion periods. It is noticeable that the well-differentiated behavior observed depends on the RC/GO ratio at short immersion periods. This suggests that the larger amount of GO involves the worst corrosion properties of the films, perhaps because of certain agglomeration of the particles. In addition, the interaction with gallic acid leads to a larger amount of rGO when the RC/GO ratio is higher, which can accelerate the cathodic reaction and corrosion rate. Chaudhry et al. reported the harmful effect of the rGO addition to self-crosslinked polyvinyl butyral (PVB) polymer [34]. Generally, the impedance of all the RC/GO formulations tends to decrease with immersion time, except that of 1RC:0.3GO, which increases at longer exposure periods. A more detailed impedance evolution of each formulation is shown in Figure 7.

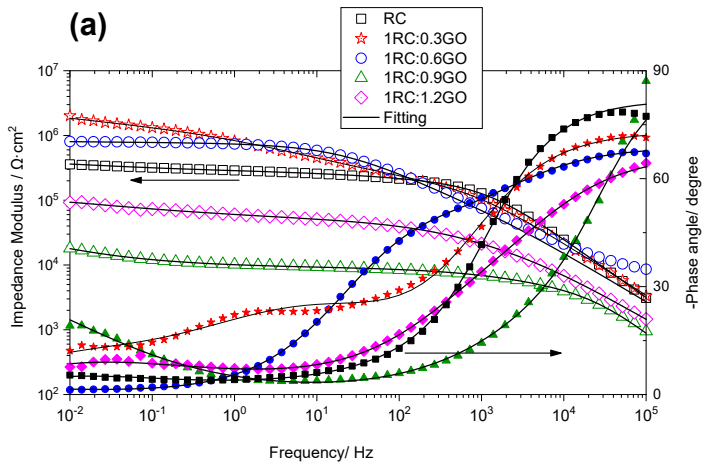


**Figure 6.** *Cont.*

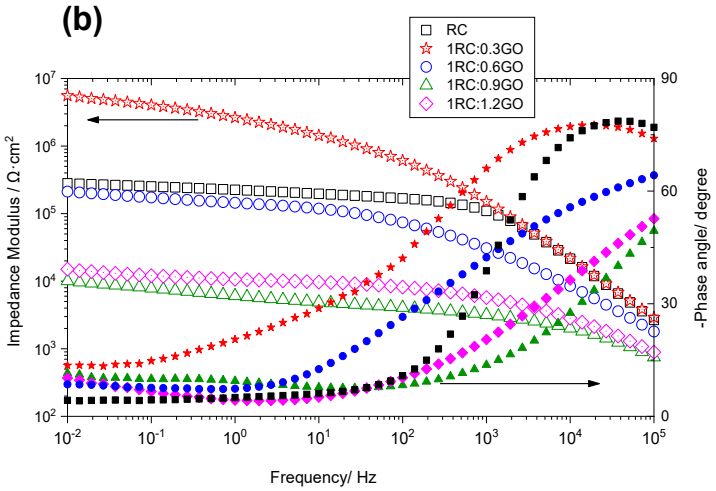


**Figure 6.** Impedance modulus (open symbols) and phase angle (filled symbols) of the rusted steel coated with the RC/GO formulations after (**a**) 4 days and (**b**) 21 days of immersion in 0.06 M NaCl solution.

As aforementioned, only 1RC:0.3GO formulation provides lasting corrosion resistance, even acquiring higher impedance values at the end of the immersion period. The complexity of the Nyquist plots suggests the emergence of several processes. The electrical equivalent circuit (EEC) used to model the observed behavior is shown in Figure 7f. In this, $R_e$ denotes the electrolyte resistance. The high-frequency time constant, $R_fC_f$, is related to the barrier properties of the conversion coating. The time constant located at the medium frequency range, $R_{ct}C_{dl}$, accounts for the charge transfer resistance and double layer capacitance of the corrosion process. Both time constants are affected by Cole–Cole type dispersion ($\alpha_f$ and $\alpha_{dl}$) [35]. The low-frequency time constant, $Z_d$, can be attributed to the oxygen diffusion toward the metallic surface. This physical interpretation is previously given in other works [36]. The total impedance is given in Equation (1):

$$Z(\omega) = R_e + \frac{R_f}{(j\omega R_f C_f)^{\alpha_f} + \frac{1}{1+Z_2/R_f}}, \quad (1)$$

The $Z_2(\omega)$ impedance is given by Equation (2):

$$Z_2(\omega) = \frac{R_{ct}}{(j\omega R_{ct} C_{dl})^{\alpha_{dl}} + \frac{1}{1+Z_d/R_{ct}}}, \quad (2)$$

Additionally, $Z_d(\omega)$ is:

$$Z_d(\omega) = R_d \frac{\tanh\sqrt{(j\omega\tau_d)}}{\sqrt{(j\omega\tau_d)}}, \quad (3)$$

In Equation (3), $Z_d(\omega)$ corresponds to semi-infinite diffusion process with a characteristic time constant $\tau_d = \delta^2/D$, where $\delta$ is the thickness of the Nernst diffusion layer, defined by the concentration gradient established by the oxygen consumption at the metal/film interface, and D accounts for the diffusion coefficient of oxygen [37]. The good agreement between the fitting and experimental data can be seen in Figures 6a and 7a–e.

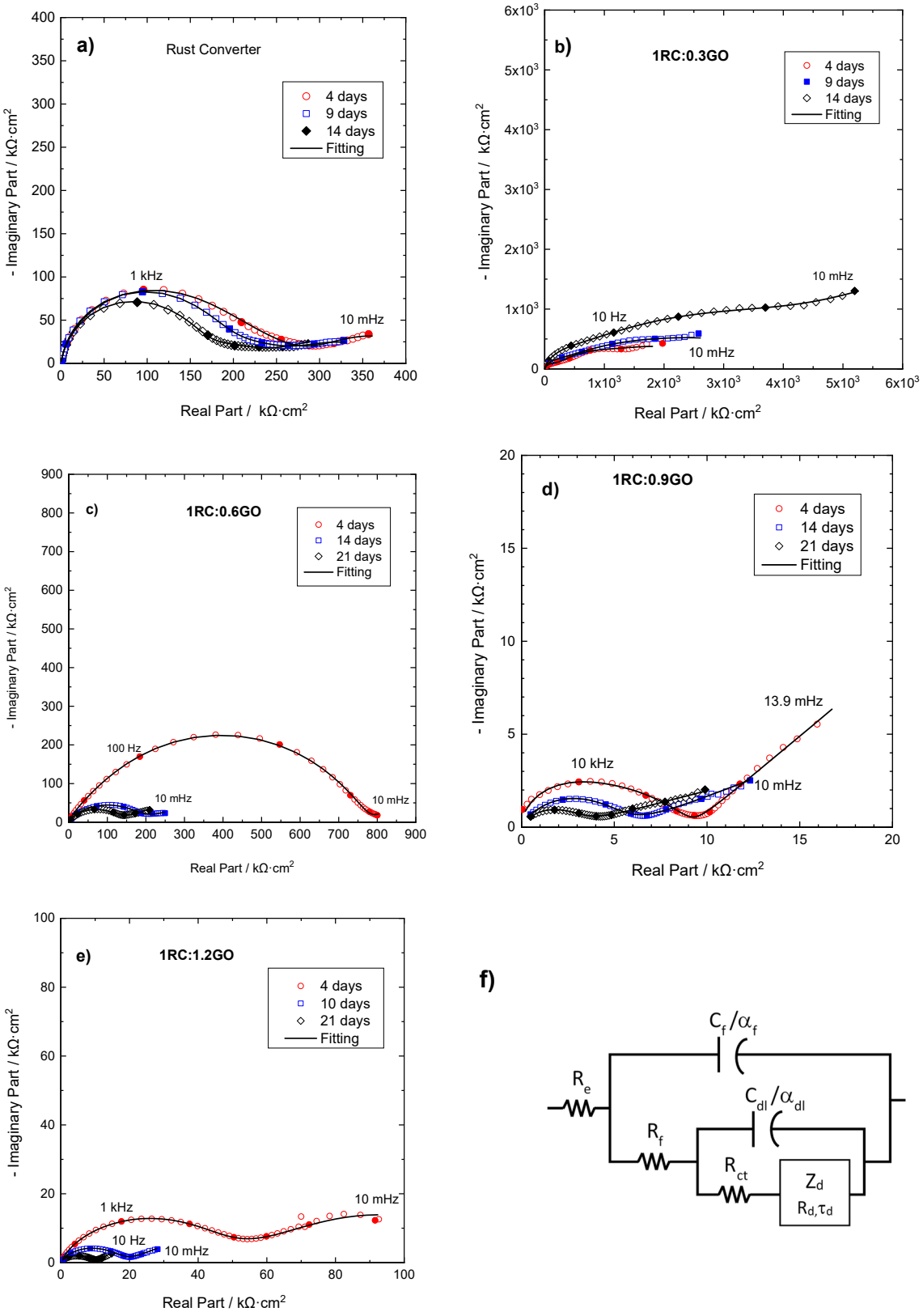


**Figure 7.** (**a**–**e**) Nyquist plots showing the evolution of the different RC/GO formulations with immersion time. The best-fit curve obtained for each measurement is also shown. (**f**) Electrical equivalent circuit (EEC) used for modeling the data. The meaning of the different elements is described in the text.

Figure 8a,b shows the evolution of the high-frequency time constant, $R_fC_f$, as aforementioned is related to the barrier properties of the conversion coating. The higher resistance values correspond to 1RC:0.3GO, followed by the undoped RC system. Initially, the 1RC:0.6GO formulation also exhibits high resistance values; however, these rapidly decrease with immersion time. On the other side, the 1RC:0.9GO and 1RC:1.2GO ratios have about one order of magnitude lower resistance values. These results illustrate the benefit afforded by small additions of GO; it seems that the conversion coatings can be effectively formed and, additionally, the GO improves the barrier effect owing to its 2D structure. As the amount of GO increases, less gallic acid (the reactive component of the RC) is available to react with the iron oxides/hydroxides, thus generating a more defective conversion coating. Parallel to the resistance evolution, the film capacitance increase observed for 1RC:0.6GO, 1RC:0.9GO, and 1RC:1.2GO formulations indicates the higher water uptake in the coating. The steady capacitance values exhibited by the other ratios corroborate the generation of a more compact layer.

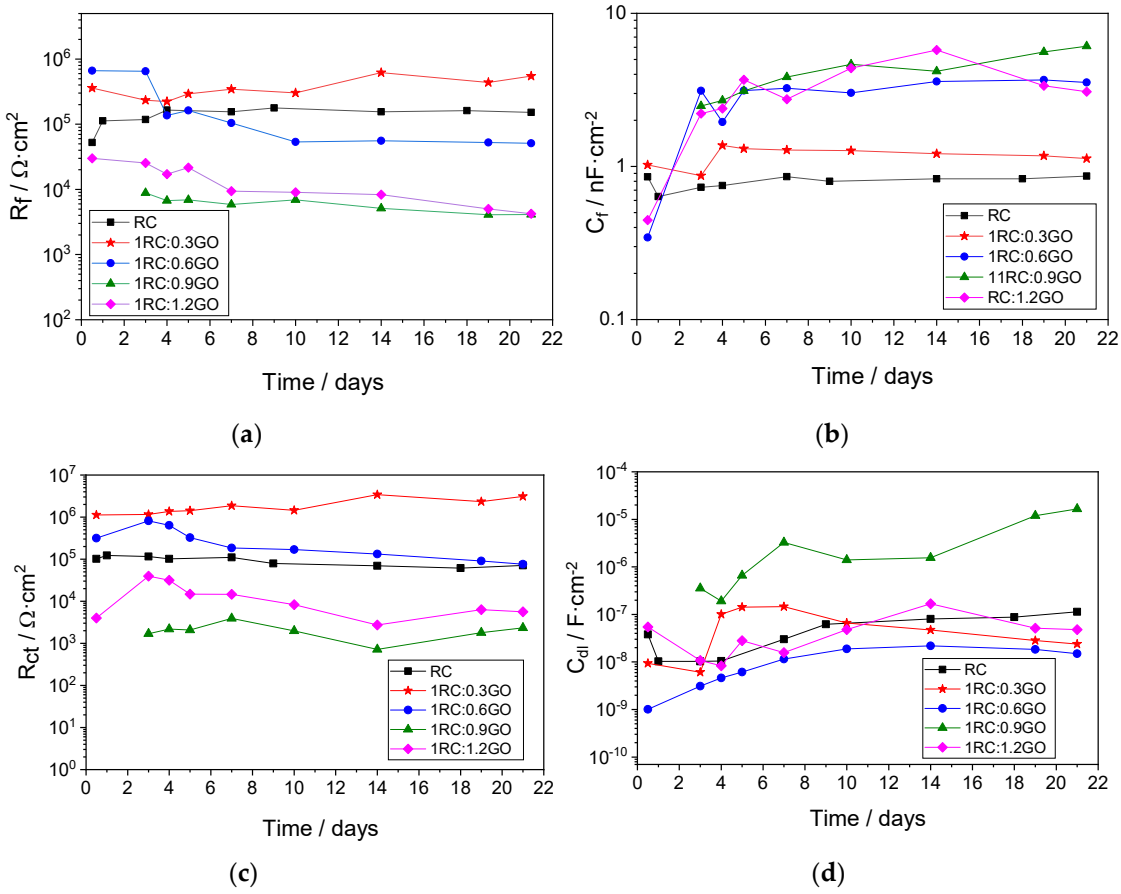


**Figure 8.** Evolution of the fitting parameters corresponding to the high-frequency time constant (**a**) $R_f$ and (**b**) $C_f$, and to the middle frequency time constant (**c**) $R_{ct}$ and (**d**) $C_{dl}$.

The evolution of the time constant associated with the corrosion process, $R_{ct}C_{dl}$, is shown in Figure 8c,d. The higher charge transfer means the lower corrosion rate [38], which corresponds to the 1RC:0.3GO system. As expected, higher corrosion rates are observed in 1RC:0.9GO and 1RC:1.2GO formulations. The double layer capacitance can be correlated to the active area, $A_d$, according to Equation (4) [39]:

$$A_d = \frac{C_{dl}}{C_{dl}^o}, \quad (4)$$

where $C_{dl}^{o}$ is the specific double layer capacitance of the bare metal, which is considered constant over the immersion time. Accordingly, $C_{dl}$ is a measure of the active area that, as can be seen in Figure 8d, increases with immersion time in all samples. However, performing an estimation of $A_d$ is not easy for rusted samples, since the value of $C_{dl}^{o}$ depends on the surface roughness. In the present study, 160 $\mu F \cdot cm^{-2}$ was adopted, which is characteristic of a very rough metallic surface [40]. The active area resulted to be less than 0.1% for all systems except 1RC:0.9GO with a larger active area (about 10%), in agreement with a lower charge transfer resistance.

It is worth commenting about the $R_{ct}$ and $C_{dl}$ values for the 1RC:0.6GO system. Although the conversion layer seems to have lower barrier properties than the undoped RC, the corrosion rate and the active surface are lower, perhaps because of the electrolyte uptakes to the film, although it does not reach the metal surface.

As aforementioned, the low-frequency time constant accounts for the oxygen diffusion transport from the bulk solution, through the layer pores, to the cathodic sites. The evolution of the associated resistance is depicted in Figure 9a. As can be seen, its evolution follows approximately the pattern observed for charge transfer resistance, the higher values correspond to the 1RC:0.3GO formulation and the lowest to the 1RC:9.9GO and 1RC:1.2GO ratios. This tendency corroborates the benefit provided by small GO additions to the RC, mainly the 1RC:0.3GO ratio.

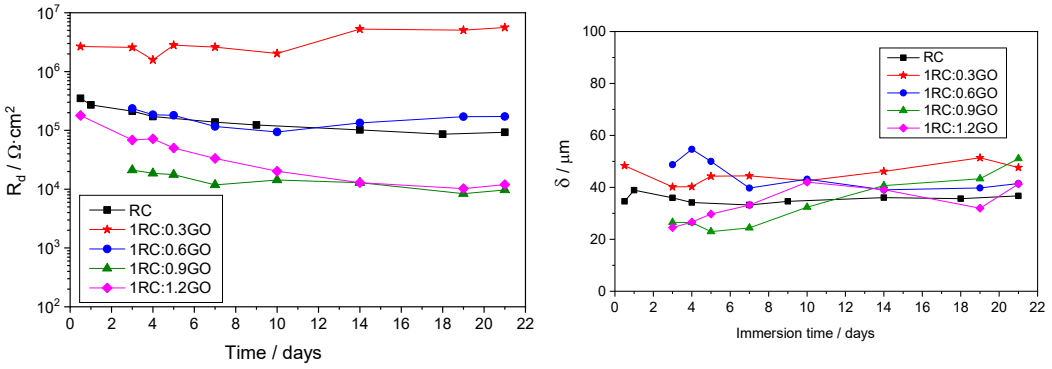


(**a**) (**b**)

**Figure 9.** Evolution with the immersion time of (**a**) $R_d$ and (**b**) the diffusion length δ.

The diffusion time constant, $\tau_d$, relates the diffusion coefficient, D, with the oxygen diffusion length, δ, by the expression $\tau_d = \delta^2/D$, previously mentioned. Assuming a typical value for oxygen diffusion through a polymer about $10^{-7}$ $cm^2 \cdot s^{-1}$ [41], estimation of δ can be performed. The results are shown in Figure 9. As can be seen, roughly the diffusion length corresponds to the conversion layer thickness, although certain fluctuation is observed, indicative of the dynamic nature of the process.

## 4. Conclusions

Different amounts of GO were added to a commercial RC in order to assess the optimum formulation range. Based on the results obtained, the following conclusions can be drawn:

The interaction between the gallic acid and the GO led to a decrease in the surface charge of the GO particles, even though the zeta-potential values confirm the stability of the colloidal suspensions for all the RC:GO ratios. This interaction was also corroborated by XRD, where the intensity of the peaks corresponding to the gallic acid markedly decreased at higher RC:GO ratios.

Additionally, the XRD technique was used to identify the main crystalline oxide/hydroxide compounds obtained from the rusted steel. They were lepidocrocite γ-FeO(OH)

and magnetite $Fe_3O_4$. The intensity of the peaks for both species strongly decreased when they were in contact with the RC.

The comparative study of the protection properties of all formulations applied on rusted steel was performed by EIS. Generally, the impedance decreased with immersion time; the only exception was the 1RC:0.3GO ratio, in which impedance values increased with time. On the other hand, lower impedance values were obtained for 1RC:0.9GO and 1RC:1.2GO ratios.

The electrical equivalent circuit used to model the observed behavior included three time constants. The high-frequency time constant was correlated to the dielectric properties of the conversion layer, the middle-frequency time constant accounted for the corrosion process, and the low-frequency time constant was associated with the oxygen diffusion through the layer pores.

Better behavior was observed for 1RC:0.3GO ratio, followed by the 1RC:0.6GO formulation. The benefit provided by the addition of small amounts of GO can be explained by taking into account its 2D morphology that increases the barrier properties. Additionally, the gallic acid may partially reduce the GO (rGO), which has hydrophobic character. If the GO amount is too high, agglomeration problems can arise, generating a more porous layer. On the other hand, the presence of higher amounts of rGO provides a major cathodic surface, which can accelerate the corrosion process.

**Author Contributions:** Conceptualization, C.P. and X.R.N.; methodology, B.D. and M.R.-M.; formal analysis, B.D. and X.R.N.; investigation, C.P. and M.R.-M.; resources, B.D. and M.R.-M.; writing—original draft preparation, C.P. and X.R.N.; writing—review and editing, C.P.; supervision, X.R.N. All authors have read and agreed to the published version of the manuscript.

**Funding:** This research received no external funding.

**Institutional Review Board Statement:** Not applicable.

**Informed Consent Statement:** Not applicable.

**Data Availability Statement:** All the data generated during this study are included in this article.

**Conflicts of Interest:** The authors declare no conflict of interest.

## References

1. Ocampo, L.M.; Margarit, I.C.P.; Mattos, O.R.; Córdoba-de-Torresi, S.I.; Fragata, F.L. Performance of rust converter based in phosphoric and tannic acids. *Corros. Sci.* **2004**, *46*, 1515–1525. [CrossRef]
2. Feliu, S.; Galván, J.C.; Feliu, S.; Bastidas, J.M.; Simancas, J.; Morcillo, M.; Almeida, E.M. An electrochemical impedance study of the behaviour of some pretreatments applied to rusted steel surfaces. *Corros. Sci.* **1993**, *35*, 1351–1358. [CrossRef]
3. Saji, V.S. Progress in rust converters. *Prog. Org. Coat.* **2019**, *127*, 88–99. [CrossRef]
4. Morcillo, M.; Feliu, S.; Simancas, J.; Bastidas, J.M.; Galvan, J.C.; Feliu, S.; Almeida, E.M. Corrosion of Rusted Steel in Aqueous Solutions of Tannic Acid. *Corrosion* **1992**, *48*, 1032–1039. [CrossRef]
5. Nasrazadani, S. The application of infrared spectroscopy to a study of phosphoric and tannic acids interactions with magnetite ($Fe_3O_4$), goethite (α-FEOOH) and lepidocrocite (γ-FeOOH). *Corros. Sci.* **1997**, *39*, 1845–1859. [CrossRef]
6. Qian, B.; Hou, B.; Zheng, M. The inhibition effect of tannic acid on mild steel corrosion in seawater wet/dry cyclic conditions. *Corros. Sci.* **2013**, *72*, 1–9. [CrossRef]
7. Gust, J. Application of infrared spectroscopy for investigation of rust phase component conversion by agents containing oak tannin and phosphoric acid Indexed keywords. *Corrosion.* **1991**, *47*, 453–457. [CrossRef]
8. Rahim, A.A.; Rocca, E.; Steinmetz, J.; Jain Kassim, M. Inhibitive action of mangrove tannins and phosphoric acid on pre-rusted steel via electrochemical methods. *Corros. Sci.* **2008**, *50*, 1546–1550. [CrossRef]
9. Jia, Y.; Ren, N.; Yue, H.; Deng, J.; Liu, Y. Preparation and properties of natural gallic acid based rust conversion emulsion. *Pigment Resin Technol.* **2016**, *45*, 191–198. [CrossRef]
10. Wang, X.; Zhu, Q.; Liu, X.; Hou, B. Rust Conversion Performance of Phosphoric Acid-Gallic Acid in Vinyl Chloride Acrylic Emulsion. *Coatings* **2021**, *11*, 152. [CrossRef]
11. Díaz, B.; Figueroa, R.; Nóvoa, X.R.; Pérez, C.; Pintos, A. The corrosion protection afforded by a commercial rust converter doped with graphene oxide. *Electrochim. Acta* **2020**, *342*, 136096. [CrossRef]
12. Xu, W.; Han, E.H.; Wang, Z. Effect of tannic acid on corrosion behavior of carbon steel in NaCl solution. *J. Mater. Sci. Technol.* **2019**, *35*, 64–75. [CrossRef]

13. Collazo, A.; Nóvoa, X.R.R.; Pérez, C.; Puga, B. EIS study of the rust converter effectiveness under different conditions. *Electrochim. Acta* **2008**, *53*, 7565–7574. [CrossRef]
14. Barrero, C.A.; Ocampo, L.M.; Arroyave, C.E. Possible improvements in the action of some rust converters. *Corros. Sci.* **2001**, *43*, 1003–1018. [CrossRef]
15. Favre, M.; Landolt, D. The influence of gallic acid on the reduction of rust on painted steel surfaces. *Corros. Sci.* **1993**, *34*, 1481–1494. [CrossRef]
16. Gust, J.; Bobrowicz, J. Sealing and Anti-Corrosive Action of Tannin Rust Converters. *Corrosion* **1993**, *49*, 24–30. [CrossRef]
17. Favre, M.; Landolt, D.; Hoffman, K.; Stratmann, M. Influence of gallic acid on the phase transformation in iron oxide layers below organic coatings studied with Moessbauer spectroscopy. *Corros. Sci.* **1998**, *40*, 793–803. [CrossRef]
18. Galván, J.C.; Simancas, J.; Morcillo, M.; Bastidas, J.M.; Almeida, E.; Feliu, S. Effect of treatment with tannic, gallic and phosphoric acids on the electrochemical behaviour of rusted steel. *Electrochim. Acta* **1992**, *37*, 1983–1985. [CrossRef]
19. Li, J.; Ge, S.; Wang, J.; Du, H.; Song, K.; Fei, Z.; Shao, Q.; Guo, Z. Water-based rust converter and its polymer composites for surface anticorrosion. *Colloids Surfaces A Physicochem. Eng. Asp.* **2018**, *537*, 334–342. [CrossRef]
20. Xue, B.; Yu, M.; Liu, J.; Li, S.; Xiong, L.; Kong, X. Corrosion Protective Properties of Silane Functionalized Graphene Oxide Film on AA2024-T3 Aluminum Alloy. *J. Electrochem. Soc.* **2016**, *163*, C798–C806. [CrossRef]
21. Ramezanzadeh, B.; Niroumandrad, S.; Ahmadi, A.; Mahdavian, M.; Mohamadzadeh Moghadam, M.H. Enhancement of barrier and corrosion protection performance of an epoxy coating through wet transfer of amino functionalized graphene oxide. *Corros. Sci.* **2016**, *103*, 283–304. [CrossRef]
22. Yu, Z.; Di, H.; Ma, Y.; He, Y.; Liang, L.; Lv, L.; Ran, X.; Pan, Y.; Luo, Z. Preparation of graphene oxide modified by titanium dioxide to enhance the anti-corrosion performance of epoxy coatings. *Surf. Coat. Technol.* **2015**, *276*, 471–478. [CrossRef]
23. Cui, J.; Xiong, Z.; Qiu, H.; LI, J.; Yang, J. Functionalized graphene oxide: Carrier for corrosion inhibitor and barrier in waterborne epoxy coatings. *Compos. Part A Appl. Sci. Manuf.* **2021**, *144*, 106354. [CrossRef]
24. Li, M.J.; Liu, C.M.; Xie, Y.B.; Cao, H.B.; Zhao, H.; Zhang, Y. The evolution of surface charge on graphene oxide during the reduction and its application in electroanalysis. *Carbon N. Y.* **2014**, *66*, 302–311. [CrossRef]
25. Hu, X.; Yu, Y.; Hou, W.; Zhou, J.; Song, L. Effects of particle size and pH value on the hydrophilicity of graphene oxide. *Appl. Surf. Sci.* **2013**, *273*, 118–121. [CrossRef]
26. Lunardi, C.N.; Gomes, A.J.; Rocha, F.S.; De Tommaso, J.; Patience, G.S. Experimental methods in chemical engineering: Zeta potential. *Can. J. Chem. Eng.* **2021**, *99*, 627–639. [CrossRef]
27. Li, J.; Xiao, G.; Chen, C.; Li, R.; Yan, D. Superior dispersions of reduced graphene oxide synthesized by using gallic acid as a reductant and stabilizer. *J. Mater. Chem. A* **2013**, *1*, 1481–1487. [CrossRef]
28. Lei, Y.; Tang, Z.; Liao, R.; Guo, B. Hydrolysable tannin as environmentally friendly reducer and stabilizer for graphene oxide. *Green Chem.* **2011**, *13*, 1655–1658. [CrossRef]
29. Ross, T.K.; Francis, R.A. The treatment of rusted steel with mimosa tannin. *Corros. Sci.* **1978**, *18*, 351–361. [CrossRef]
30. de la Fuente, D.; Díaz, I.; Simancas, J.; Chico, B.; Morcillo, M. Long-term atmospheric corrosion of mild steel. *Corros. Sci.* **2011**, *53*, 604–617. [CrossRef]
31. Chen, Y.H.; Li, F.A. Kinetic study on removal of copper(II) using goethite and hematite nano-photocatalysts. *J. Colloid Interface Sci.* **2010**, *347*, 277–281. [CrossRef] [PubMed]
32. Compeán-Jasso, M.E.; Ruiz, F.; Martínez, J.R.; Herrera-Gómez, A. Magnetic properties of magnetite nanoparticles synthesized by forced hydrolysis. *Mater. Lett.* **2008**, *62*, 4248–4250. [CrossRef]
33. Antony, H.; Legrand, L.; Maréchal, L.; Perrin, S.; Dillmann, P.; Chaussé, A. Study of lepidocrocite γ-FeOOH electrochemical reduction in neutral and slightly alkaline solutions at 25 °C. *Electrochim. Acta* **2005**, *51*, 745–753. [CrossRef]
34. Chaudhry, A.U.; Mittal, V.; Mishra, B. Inhibition and promotion of electrochemical reactions by graphene in organic coatings. *RSC Adv.* **2015**, *5*, 80365–80368. [CrossRef]
35. MacDonald, J.R. *Impedance Spectroscopy: Emphasizing Solid Materials and Systems*; John Wiley & Sons, Inc.: New York, NY, USA, 1987; ISBN 0-471-83122-0.
36. Pérez, C.; Collazo, A.; Izquierdo, M.; Merino, P.; Nóvoa, X.R. Electrochemical impedance spectroscopy study of the corrosion process on coated galvanized steel in a salt spray fog chamber. *Corrosion* **2000**, *56*, 1220–1232. [CrossRef]
37. Amirudin, A.; Thierry, D. Application of electrochemical impedance spectroscopy to study the degradation of polymer-coated metals. *Prog. Org. Coat.* **1995**, *26*, 1–28. [CrossRef]
38. Lorenz, W.J.; Mansfeld, F. Determination of corrosion rates by electrochemical DC and AC methods. *Corros. Sci.* **1981**, *21*, 647–672. [CrossRef]
39. McIntyre, J.M.; Pham, H.Q. Electrochemical impedance spectroscopy; a tool for organic coatings optimizations. *Prog. Org. Coat.* **1996**, *27*, 201–207. [CrossRef]
40. Cabanelas, I.; Collazo, A.; Izquierdo, M.; Nóvoa, X.R.; Pérez, C. Influence of galvanised surface state on the duplex systems behaviour. *Corros. Sci.* **2007**, *49*, 1816–1832. [CrossRef]
41. Thomas, N.L. The Barrier Properties of Paint Coatings. *Prog. Org. Coat.* **1991**, *19*, 101–121. [CrossRef]